Article

Cell Systems

Growth-Optimized Aminoacyl-tRNA Synthetase Levels Prevent Maximal tRNA Charging

Graphical Abstract

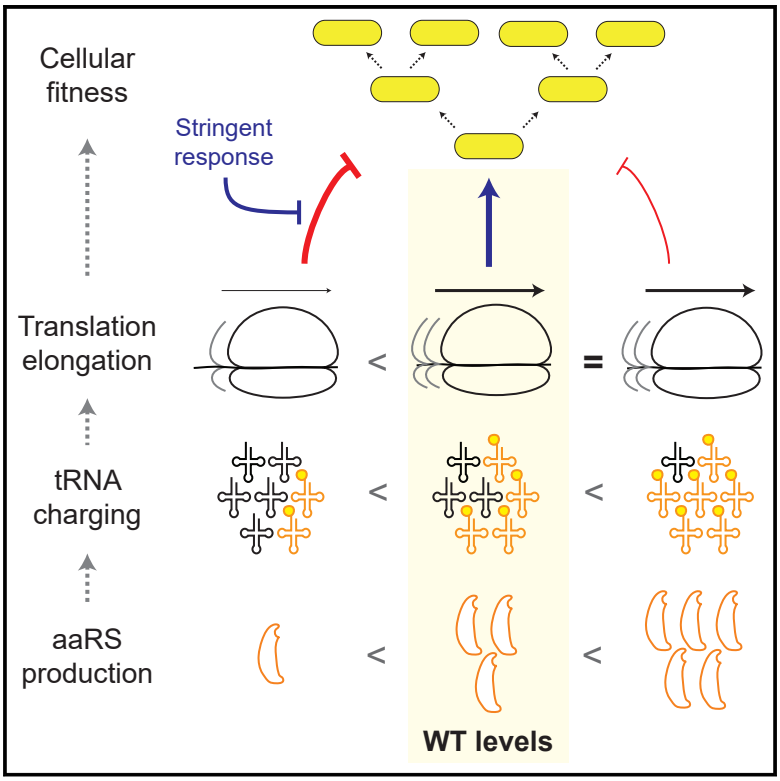

Authors

Darren J. Parker, Jean-Benoît Lalanne, Satoshi Kimura, Grace E. Johnson, Matthew K. Waldor, Gene-Wei Li

Correspondence

gwli@mit.edu

In Brief

An integrated analysis of tRNA charging, translation elongation, and bacterial growth rates reveals that the production of aminoacyl-tRNA synthetases is growth-optimized atop a "fitness cliff" in *Bacillus subtilis*. The optimized production rates satisfy the flux required for peptide chain elongation without minimizing the levels of uncharged tRNAs, whose detrimental effects are alleviated by precisely tuned stringent response and autoregulation.

Highlights

- Bacteria produce just enough aaRSs to support the amino acid fluxes for translation
- tRNA charging is not maximized at growth-optimized levels of aaRS production
- Native levels of uncharged tRNAs have limited impacts on cell fitness
- Stringent response alleviates fitness defects of aaRS underproduction in rich media

Parker et al., 2020, Cell Systems *11*, 1–10
August 26, 2020
https://doi.org/10.1016/j.cels.2020.07.005

CellPress

Please cite this article in press as: Parker et al., Growth-Optimized Aminoacyl-tRNA Synthetase Levels Prevent Maximal tRNA Charging, Cell Systems (2020), https://doi.org/10.1016/j.cels.2020.07.005

Cell Systems

CellPress

Article

Growth-Optimized Aminoacyl-tRNA Synthetase Levels Prevent Maximal tRNA Charging

Darren J. Parker,[1] Jean-Benoît Lalanne,[1,2] Satoshi Kimura,[3,4,5] Grace E. Johnson,[1] Matthew K. Waldor,[3,4,5] and Gene-Wei Li[1,6,*]

[1]Department of Biology, Massachusetts Institute of Technology, Cambridge, MA 02139, USA
[2]Department of Physics, Massachusetts Institute of Technology, Cambridge, MA 02139, USA
[3]Division of Infectious Diseases, Brigham and Women's Hospital, Boston, MA 02115, USA
[4]Department of Microbiology, Harvard Medical School, Boston, MA 02115, USA
[5]Howard Hughes Medical Institute, Harvard Medical School, Boston, MA 02115, USA
[6]Lead Contact
*Correspondence: gwli@mit.edu
https://doi.org/10.1016/j.cels.2020.07.005

SUMMARY

Aminoacyl-tRNA synthetases (aaRSs) serve a dual role in charging tRNAs. Their enzymatic activities both provide protein synthesis flux and reduce uncharged tRNA levels. Although uncharged tRNAs can negatively impact bacterial growth, substantial concentrations of tRNAs remain deacylated even under nutrient-rich conditions. Here, we show that tRNA charging in *Bacillus subtilis* is not maximized due to optimization of aaRS production during rapid growth, which prioritizes demands in protein synthesis over charging levels. The presence of uncharged tRNAs is alleviated by precisely tuned translation kinetics and the stringent response, both insensitive to aaRS overproduction but sharply responsive to underproduction, allowing for just enough aaRS production atop a "fitness cliff." Notably, we find that the stringent response mitigates fitness defects at all aaRS underproduction levels even without external starvation. Thus, adherence to minimal, flux-satisfying protein production drives limited tRNA charging and provides a basis for the sensitivity and setpoints of an integrated growth-control network.

INTRODUCTION

Aminoacyl-tRNA synthetases (aaRS) catalyze a universal step in the synthesis of proteins by ligating amino acids to the appropriate tRNA, a process termed "tRNA charging." Their enzymatic activities determine two interrelated but distinct properties: the flux of charged tRNAs to the ribosome and the steady-state levels of uncharged tRNAs, both of which are important for regulating cell growth (Figure 1A). First, the flux of tRNA aminoacylation is directly related to the overall rate of peptide chain growth and hence the rates of mass accumulation and growth in bacteria (Bremer and Dennis, 2008; Dai et al., 2016). Second, the steady-state level of charged (acylated) tRNAs is inversely related to the level of uncharged (deacylated) tRNAs, which have several negative effects on cell physiology. On a global scale, uncharged tRNAs trigger stress responses that slow down cell growth in both bacteria and eukaryotes (Hinnebusch, 2005; Potrykus and Cashel, 2008; Srivatsan and Wang, 2008). In bacteria, uncharged tRNA levels are sensed by the (p)ppGpp synthetase RelA, whose activity reduces growth via a variety of pathways collectively referred to as the stringent response (Gourse et al., 2018; Hauryliuk et al., 2015; Liu et al., 2015). On the molecular scale, reduced tRNA charging is thought to cause ribosome pausing, which has adverse effects on mRNA stability and co-translational protein folding (Gloge et al., 2014; Hanson and Coller, 2018; Rauscher and Ignatova, 2018). Given the importance of aaRS's dual roles, it is plausible that aaRS production is tuned to both minimize uncharged tRNA levels and provide ample capacity for charging flux during rapid cell growth.

However, a substantial concentration of uncharged tRNAs has been frequently observed *in vivo* even under rich nutrient conditions across divergent bacteria (Avcilar-Kucukgoze et al., 2016; Dittmar et al., 2005; McClain et al., 1999; Tockman and Vold, 1977; Yegian et al., 1966). For a wide spectrum of tRNAs—both within the same organism as well as across divergent bacterial species, the concentrations of uncharged tRNAs and total tRNAs are close to the same order of magnitude. This is despite the fact that the production of many aaRSs is directly set by uncharged tRNA levels (and not charging flux) via various negative autoregulatory mechanisms (Giegé and Springer, 2016; Gutiérrez-Preciado et al., 2009; Putzer et al., 1995; Vitreschak et al., 2008), suggesting that the setpoints of these feedback loops have evolved to avoid high levels of aaRSs and low levels of uncharged tRNAs. The potential tension between high concentrations of uncharged tRNA and their pleiotropic effects points to a global optimization problem of aaRS production that prevents maximal tRNA charging by cells.

Please cite this article in press as: Parker et al., Growth-Optimized Aminoacyl-tRNA Synthetase Levels Prevent Maximal tRNA Charging, Cell Systems (2020), https://doi.org/10.1016/j.cels.2020.07.005

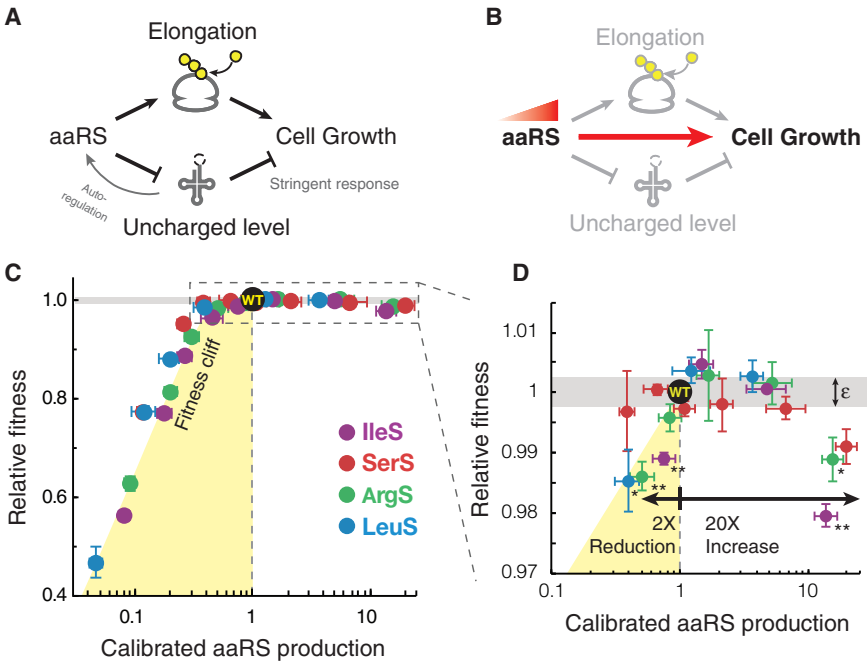

Figure 1. Fitness Landscape of tRNA Synthetase Production Shows Growth Optimization Near a Fitness Cliff

(A) Model describing the dual roles of aminoacyl-tRNA synthetase (aaRS) concentrations and their relation to the cellular growth rate (black lines). The production of aaRS is subject to negative feedback regulation by uncharged tRNAs in *Bacillus subtilis* (gray line).

(B) Fitness landscape defined as the effective relationship between aaRS production and exponential-phase population growth rate. To measure the fitness landscape, we removed the negative feedback regulation to allow direct control of aaRS production.

(C) Empirical fitness landscape of aaRS production. For each aaRS, gene expression is tuned by IPTG, and the effective protein production is calibrated to its native levels using a method based on ribosome profiling (STAR Methods). Relative fitness is defined as the relative growth rate compared with barcoded control strains in pooled competition experiments. Yellow-shaded regions indicate the approximate location of the fitness cliff. Error bars indicate standard error of fitness measurements for individually barcoded, biological replicates. Gray area indicates experimental uncertainty in fitness values relative to wild type (ε = 0.5%). (D) Empirical fitness landscape of aaRS production near wild-type fitness levels. Asterisks indicate p value < 0.05 (one asterisk) and <0.01 (two asterisks) from two-sample one-tailed Student's t test comparing barcoded replicates between control and aaRS induction experiment. See also Figure S1.

Understanding this potential optimization in aminoacylation requires a systems-level characterization of the molecular and physiological consequences of altering aaRS production rates. A priori, it is unclear whether charging levels are sensitive to small perturbations in aaRS production, as multiple enzymes have been shown to be produced with excess capacities (Davidi and Milo, 2017; O'Brien et al., 2016; Peters et al., 2016; Sander et al., 2019). tRNA charging levels could potentially be increased with aaRS overproduction, but whether or not this leads to faster translation elongation depends on additional biochemical parameters *in vivo*, such as the kinetics of ribosome translocation and availability of EF-Tu. Furthermore, elevated aaRS production may incur benefit-offsetting burdens on cell fitness, including cost of synthesis or synthetase-specific overproduction defects (Dekel and Alon, 2005; Dong et al., 1995; Scott and Hwa, 2011; Sherman et al., 1992; Swanson et al., 1988). These considerations contribute to the fitness landscape of cells relative to aaRS production, which is potentially modified by the stringent response that connects growth rates to charging levels. In general, detailed quantitative relationships between protein production, biochemical activities, and phenotypic outcomes have been difficult to establish.

Here, we determined the dependency and mechanistic underpinnings of bacterial cell growth on aminoacyl-tRNA synthetase production. High-precision measurements of cellular fitness and aaRS production rates show that these proteins are produced with little excess in order to optimize the growth rate of *Bacillus subtilis* in nutrient-rich conditions. Although tRNA charging is not maximized at the growth-optimized aaRS levels, the charging capacity matches the flux required to support translation elongation. At native aaRS production levels, the substantial pool of uncharged tRNAs does not lead to pleiotropic effects, due in part to a lack of strong activation of the stringent response. Nevertheless, cells remain exquisitely sensitive to even slight aaRS underproduction despite being relatively insensitive to overproduction. Notably, although the stringent response is known for curbing growth during external amino acid starvation, we find that it partially alleviates growth defects during aaRS underproduction—a condition in which *de novo* amino acid synthesis does not provide benefits. Ribosome profiling reveals that stringent null cells display both a lack of coordination of gene expression and exacerbated translation kinetic defects during aaRS underproduction. Together, these results show that the circuits for both controlling and sensing tRNA aminoacylation are collectively tuned to optimize bacterial growth, leading to unexpected properties of cellular mechanisms that are elucidated only with a fully integrated analysis.

RESULTS

aaRS Production is Growth Optimized on an Acutely Asymmetric Landscape

We first mapped the quantitative relationship between cell proliferation rates and individual aaRS protein production in *B. subtilis*, a relationship we refer to as the fitness landscape (Figure 1B). Four essential synthetase genes were chosen as models (*argS*, *ileS*, *leuS*, and *serS*) for several key reasons. First, they reside in their own monocistronic operons, which allow for targeted perturbations. Second, these aaRSs are not heteromeric, eliminating the need to maintain stoichiometric production of multiple subunits exogenously. Third, the regulation of these genes is representative of aaRS regulation in *B. subtilis*, which includes both feedback regulation by T Box elements (*ileS*, *leuS*, and *serS*) and constitutive expression (*argS*).

Please cite this article in press as: Parker et al., Growth-Optimized Aminoacyl-tRNA Synthetase Levels Prevent Maximal tRNA Charging, Cell Systems (2020), https://doi.org/10.1016/j.cels.2020.07.005

Although it is expected that cell growth would be affected at extreme levels of aaRS underproduction, the precise mapping of aaRS production onto fitness has not been determined.

In order to systematically vary aaRS production, we first moved each gene outside its native context and placed it under the control of an IPTG-inducible promoter (Britton et al., 2002). Using this system, the effective aaRS production relative to the wild-type level ranges from 10-fold underproduction to 10-fold overproduction, as estimated by considering the IPTG-dependent promoter strength and the translation efficiency of the ectopic mRNA (measured by ribosome profiling) (Figure S1A; STAR Methods). At each IPTG concentration, the competitive disadvantage during exponential growth was measured using a pooled competition assay with DNA barcoding, which can reliably detect 0.5% differences in the net steady-state growth rate (Figure S1B). Fitness for aaRS inducible strains is defined as the growth rate compared with barcoded control strains with the same antibiotic resistance markers. The combination of these methods provides a generalizable approach for mapping the precise dependence of fitness on individual protein production.

The fitness landscapes for all synthetases showed a strong asymmetry between low and high levels of production (Figure 1C). At low levels of aaRS, fitness is acutely sensitive to aaRS production. This "fitness cliff" may arise from insufficient flux of tRNA charging for cell growth or premature activation of the stringent response. By contrast, fitness is much less sensitive to high levels of aaRS, which may be due to a lack of changes in tRNA charging or reduced dependence of fitness on tRNA charging. The mechanistic basis underlying these behaviors is central to understanding bacterial growth regulation and is examined in further detail below.

We found that the wild-type production rates of aaRS are growth optimized on the fitness landscape, placing cells near the edge of the fitness cliff. For all synthetases tested, no other aaRS expression level leads to a measurable increase in growth rate. Near the growth-optimized levels, cells with 2-fold less aaRS production have an average fitness defect of 1% (Figure 1D) and are steadily lost in the competition assay. In contrast, a greater than 10-fold overproduction is required to produce a similar fitness defect (Figure 1D). The observed fitness landscape is quantitatively similar across different aaRSs, including SerS whose tRNA charging levels are often low and could potentially benefit from overproduction (Avcilar-Kucukgoze et al., 2016; Dittmar et al., 2005; Ferro et al., 2017). The asymmetric sensitivity is further confirmed by measuring mass doubling times at selected inducer concentrations (Figure S1C). Despite the comparatively small fitness effects of overproduction, cells appear to produce just enough aaRS proteins, leaving limited buffering capacity for tRNA charging for each of the aaRSs. Together, the asymmetric fitness landscape surrounding the growth optimum suggests that there is a non-trivial transition in the level of tRNA charging or dynamics of mRNA translation near-native aaRS production.

aaRS Overproduction Boosts tRNA Charging Despite a Lack of Fitness Benefit

We next determined whether tRNA charging ceases to increase with aaRS overproduction, which could explain a lack of benefit in the overproduction regime (Figure 2A). Using northern blotting to quantify aminoacylated and deacylated tRNAs, we found that the charging levels in wild-type *B. subtilis* cells were between 50%–65% (Figure 2B), near the levels observed in other bacterial species (Avcilar-Kucukgoze et al., 2016; Dittmar et al., 2004; Yegian et al., 1966). For all aaRSs tested, ectopic overproduction (5- to 20-fold above native levels) increased the charging levels of cognate tRNAs, in some cases to nearly 90% (Figure 2B). These results indicate that the lack of fitness benefit beyond-native aaRS levels is not due to cessation in tRNA charging increase.

To independently confirm these results, we created reporter systems utilizing the native autoregulation for aaRS genes (Figure 2C). In *B. subtilis*, most aaRS genes have T box leader elements in their 5′ UTR, which bind to uncharged tRNA and activate transcription in a concentration-dependent manner (Green et al., 2010; Gutiérrez-Preciado et al., 2009). Taking advantage of these sensors, we fused the T Box with a gene encoding GFP at the locus that originally harbors the native copy of synthetase gene. In this broken autoregulatory system, increases in uncharged tRNA levels can be read out by increases in *gfp* expression as measured by qRT-PCR (Figure 2C). These reporters confirmed that aaRS overproduction leads to higher charging (decreased *gfp* expression) (Figure 2D). They also showed that the riboswitches (and consequently charging level) are continuously responsive to a wide range of aaRS production, i.e., both under and overproduction (Figures 2D and S2A). We note that the magnitude of changes in *gfp* expression is dependent upon the sensitivity of the T Box elements and is not a quantitative readout of uncharged tRNA levels. Together with the fitness landscape profiling, these results suggest that the benefits of reducing uncharged tRNA levels during aaRS overproduction are limited and potentially negated by other processes in the cells.

Translation Elongation is Sensitive to Decreased but Not Increased aaRS Production

We next show that a transition in translation elongation kinetics underlie the saturated growth response associated with elevated aaRS production (Figure 3A). To estimate the relative ribosome transit time at each codon, we performed ribosome profiling on wild-type cells and the inducible aaRS strains across the expression landscape. The mean ribosome occupancy for each codon accounts for the total transit time across a full elongation cycle (Wu et al., 2019), including the waiting times for ternary complex binding and ribosome translocation that determines the net rates of peptide chain synthesis and cell growth (Figure 3B).

We found that ribosome transit time is sensitive to aaRS underproduction but not overproduction. aaRS reduction leads to increased ribosome occupancy for the cognate codons (Figures 3C, S3A, and S3C) and even a 2-fold reduction from the native production rates has a noticeable effect. Although the slower growth rates in these conditions may reduce global tRNA expression, such a global decrease is not expected to lead to the amino acid specific ribosome pausing that we observed when the corresponding aaRS is underproduced. Furthermore, we found that the levels of tRNA cognate to the underproduced aaRS are not reduced compared with other tRNAs, demonstrating that decreased tRNA charging is the major mechanism leading to increased ribosome pausing (Figure S3E). Consistent

Please cite this article in press as: Parker et al., Growth-Optimized Aminoacyl-tRNA Synthetase Levels Prevent Maximal tRNA Charging, Cell Systems (2020), https://doi.org/10.1016/j.cels.2020.07.005

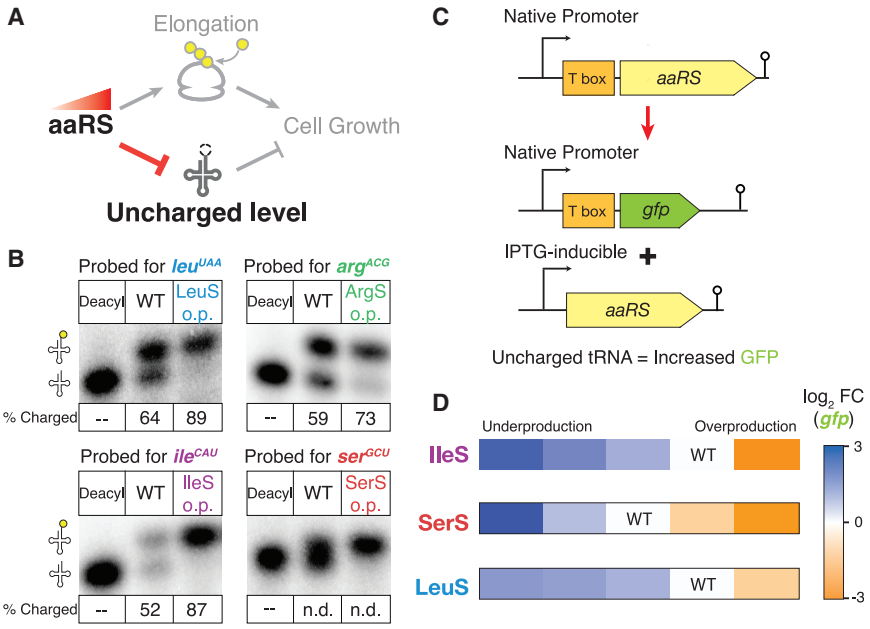

Figure 2. aaRS Overproduction Reduces Uncharged tRNA Levels

(A) Simplified relationship between aaRS production and uncharged tRNA levels. In practice, overproduction of aaRS may not reduce uncharged tRNA levels if there is already excess charging capacity at native levels of aaRS production.

(B) Representative northern blots to determine tRNA charging levels in wild type and aaRS overproduction strains. A control sample of deacylated tRNA was used to determine location of uncharged tRNAs. The middle lane of each blot contains tRNA extracted from wild-type cells (strain 168), and the final lane (o.p.) contains tRNA from aaRS induction strains with 500 μM IPTG (3.7×, 16×, 14×, and 20× overproduction for LeuS, ArgA, IleS, and SerS, respectively). Fraction of charged tRNA was calculated as the ratio between the lower band and the sum of the upper and lower band. Due to a lack of sufficient separation of aminoacylated serine tRNA, quantification was not determined (n.d.).

(C) Schematic of reporter used to measure changes in uncharged tRNA levels. The native copy of the aaRS gene was replaced with a *gfp* gene and moved under the control of an IPTG-inducible promoter (PspankHy) at the *amyE* locus in the genome.

(D) T box reporter activity over range of aaRS production. For each inducible aaRS strain, the change in uncharged tRNA levels was reported by the fold change (FC) of *gfp* compared with induction conditions with near-native aaRS production (indicated). Induction conditions with both under and over native production was tested and *gfp* mRNA measured by qRT-PCR. The native *argS* locus does not contain a T box, and therefore, was not tested in this assay. See also Figure S2.

with previous reports in the context of amino acid limitation (Elf et al., 2003; Subramaniam et al., 2013a, 2013b), we observed a hierarchy of sensitivity among the cognate codons for both LeuS and SerS, where only four of the six codons saw a substantial increase in ribosome occupancy upon aaRS reduction. Such differential sensitivity may arise from differences in the ratio of codon usage and tRNA abundance (Elf et al., 2003; Subramaniam et al., 2013a, 2013b). These results show that slower translation due to reduced charging is associated with the acute sensitivity on the fitness landscape upon aaRS underproduction.

In contrast to underproduction, aaRS overproduction does not lead to substantial changes in the elongation kinetics. For codons cognate to the inducible synthetase, we observed similar ribosome occupancy during aaRS overproduction compared with wild type (Figures 3D, S3B, and S3D), suggesting that the elongation cycle is limited by other processes or that the increase in charged tRNA levels is not sufficient to accelerate translation elongation. Although it is possible that the transit time decreases below our limit of detection, the lack of sensitivity of elongation kinetics at elevated tRNA charging levels is consistent with several lines of evidence in the literature suggesting that the ternary complex concentration is near saturation for the elongation cycle (Dai et al., 2016; Gouy and Grantham, 1980; Klumpp et al., 2013; Subramaniam et al., 2014). Consequently, elevated aaRS production has little to no benefit on translation, even though tRNA charging is increased. In addition to this limited benefit, the observed decrease in fitness with elevated aaRS production may arise from the costs associated with unnecessary protein synthesis (~2% of global protein synthesis capacity with 10-fold overproduction for individual aaRS) (Dong et al., 1995; Scott et al., 2010). Together, these results show that the wild-type levels of aaRS production are set to provide just enough capacity for supporting translational flux instead of minimizing uncharged tRNA levels.

The Stringent Response is Protective During aaRS Underproduction in Rich Media

The omnipresence of uncharged tRNAs, even at native aaRS production, suggests that (p)ppGpp, and the stringent response may play an important role in shaping the fitness landscape. The physiological consequences of the stringent response are well studied under conditions of external amino acid starvation, but how the response affects aaRS optimization under nutrient-rich conditions is unknown. Gene expression profiling by RNA sequencing across the aaRS production landscape showed signatures of elevated (p)ppGpp levels only during aaRS underproduction, including branch chain amino acid biosynthesis and CodY-controlled gene upregulation (Figures 4A and S4A) (Eymann et al., 2002; Kriel et al., 2014; Sonenshein, 2005). This upregulation was prominent despite the fact that excess amino acids are provided in the media. A major role of the stringent response during amino acid limitation is growth reduction by diverting gene expression away from genes involved in protein synthesis and toward those involved in *de novo* amino acid biosynthesis. However, since amino acids are readily available in the media, spending resources on creating biosynthetic enzymes is unnecessary and could be wasteful, thereby amplifying the effects of insufficient tRNA charging during aaRS

Please cite this article in press as: Parker et al., Growth-Optimized Aminoacyl-tRNA Synthetase Levels Prevent Maximal tRNA Charging, Cell Systems (2020), https://doi.org/10.1016/j.cels.2020.07.005

CellPress

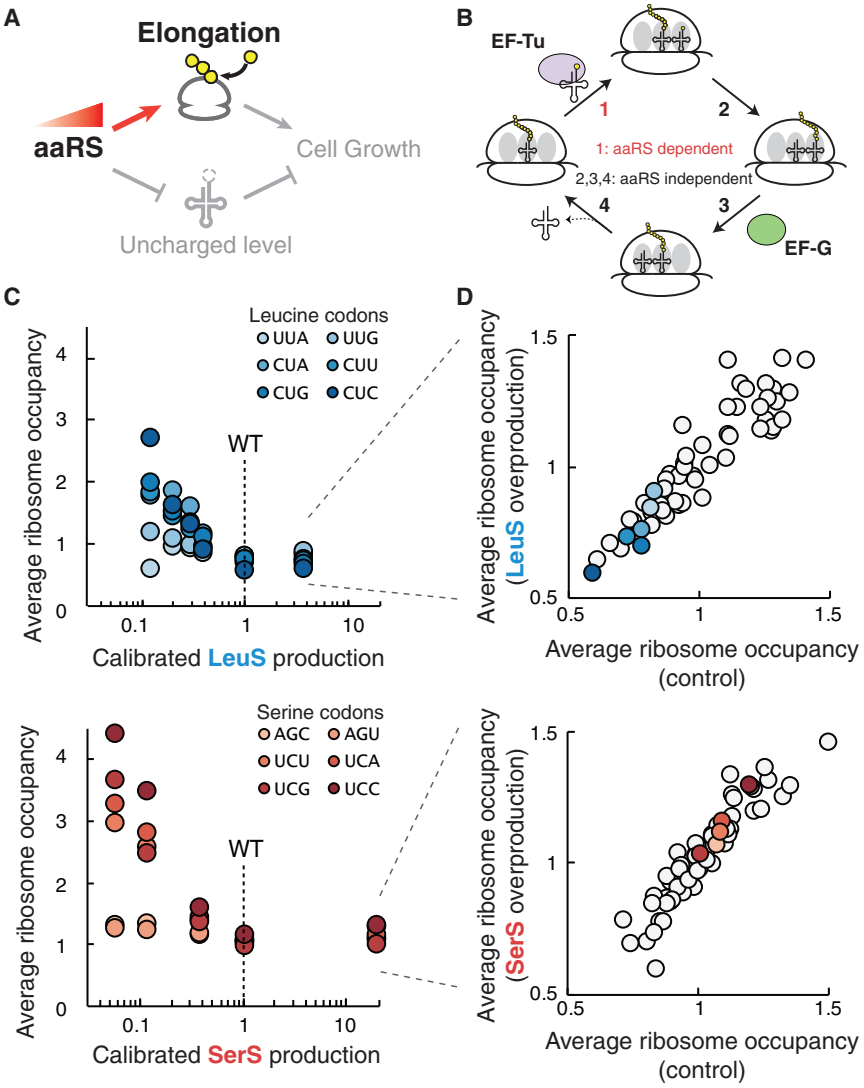

Figure 3. Translation Elongation Kinetics Change Only with aaRS Underproduction

(A) Relationship between aaRS production and translation elongation rate to be tested.

(B) Simplified schematic of the translation elongation cycle. The step of ternary complex binding (1) depends on aaRS production but may not be rate-limiting for the elongation cycle.

(C) Changes in codon occupancy across aaRS production. Average codon occupancy for indicated codons was acquired by ribosome profiling at the specific aaRS induction levels for LeuS and SerS (STAR Methods). 81 genes for LeuS induction and 218 genes for SerS induction passed the depth threshold in all experiments and were used for analysis.

(D) Average ribosome occupancy for all 61 sense codons for aaRS overproduction and control. See also Figure S3.

underproduction. Alternatively, the redistribution of resources may instead be beneficial due to reduction in ribosome production. These two models predict opposite growth effects upon removal of the stringent response (Figure 4B).

To test the effect of the stringent response on cell growth when aaRS is underproduced in rich media, we measured fitness of *B. subtilis* strains with inducible aaRS but lacking the ability to activate RelA-dependent (p)ppGpp synthesis. In these strains, we introduced a point mutation to the native copy of *relA* (*relA* D264G) that has been previously shown to abolish the (p)ppGpp synthetase activity while retaining the ability to hydrolyze background levels of (p)ppGpp, as evidenced by no detectable (p)ppGpp during serine hydroxamate treatment (Nanamiya et al., 2008). As a control, we found that this mutation has only a mild effect on growth at native aaRS levels (0.6 ± 0.3% relative fitness) and few gene expression changes (Figures S4B and S4C). However, upon aaRS underproduction, strains without the stringent response showed further exacerbated fitness cliffs as measured by the competition assay (Figure 4C). Across all aaRSs tested, removal of (p)ppGpp synthetase activity leads to an additional decrease in fitness of ~2.5% at ~2-fold aaRS underproduction and ~25% at ~10-fold underproduction. The severe growth defects were further confirmed by measuring mass doubling of individual cultures (Figure S4C). These results indicate that, instead of curtailing bacterial growth rates, the stringent response, in fact, enhances growth when there is insufficient aminoacyl-tRNA synthetase activity in the absence of external starvation.

We next characterized the molecular defects in mRNA translation associated with the reduced fitness in stringent null cells during aaRS underproduction. In *E. coli*, the stringent response enforces a linear relationship between growth rate and the production of translation-related proteins (Scott et al., 2010; Zhu and Dai, 2019), such that ribosomes are operating near capacity at most growth rates. Using ribosome profiling to quantify the allocation of global protein synthesis to translation-related factors, we found that *B. subtilis* cells with aaRS underproduction adhere to a similar linear relationship when the stringent response is present (Figure 5A). This applies to both core ribosomal proteins and translation factors, such as other aaRSs that are not externally controlled. However, the coordinated reduction is lost in cells without the stringent response, which overproduce ribosomal proteins and translation factors without matching production of supporting aaRSs (Figures 5A and S5A).

We also found that the uncoordinated production of translation machinery is accompanied with exacerbated ribosome pausing and can even lead to ribosome queuing during translation. For cells that cannot activate the stringent response, ribosome profiling data showed higher ribosome occupancy at the starved codons compared with cells with an intact stringent response (Figure 5B). In the case of SerS, underproduction leads to elevated ribosome occupancy at regularly spaced

Please cite this article in press as: Parker et al., Growth-Optimized Aminoacyl-tRNA Synthetase Levels Prevent Maximal tRNA Charging, Cell Systems (2020), https://doi.org/10.1016/j.cels.2020.07.005

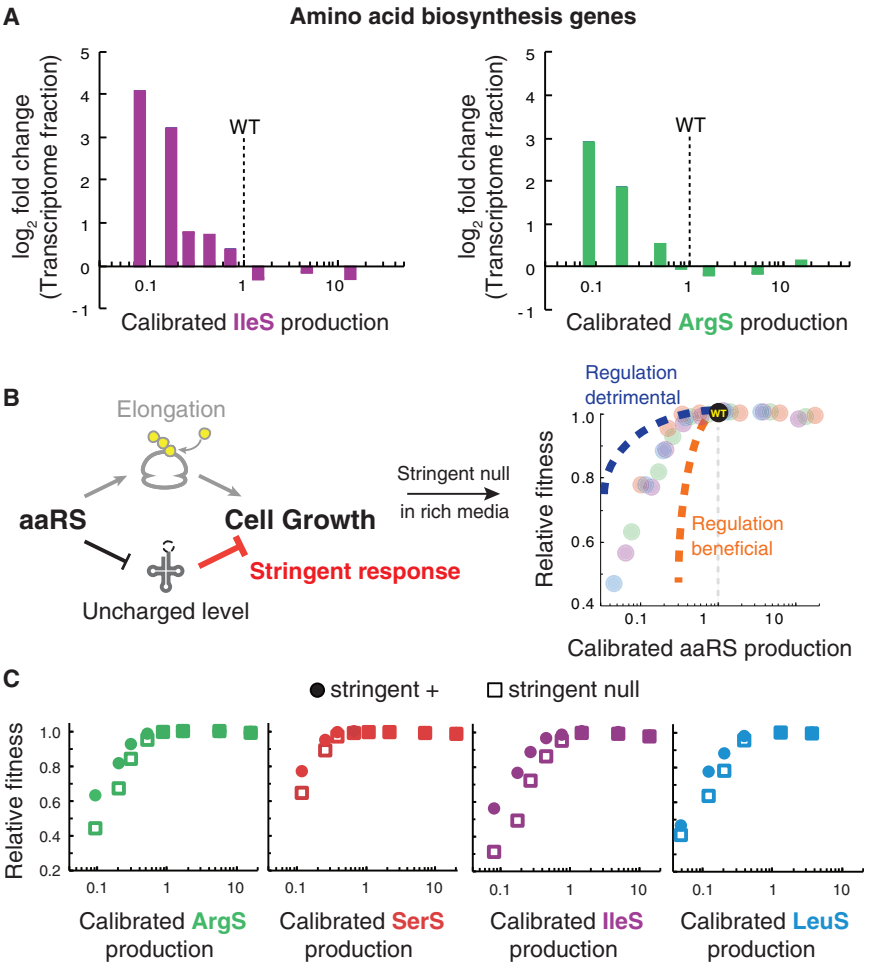

Figure 4. Removal of the Stringent Response Negatively Impacts Cell Growth during aaRS Underproduction

(A) Induction of CodY-controlled amino acid biosynthetic genes as a proxy for stringent response activation across aaRS expression. RNA-seq was performed on strains producing IleS and ArgS over a range of induction conditions. The fold change in transcriptome fraction (RPKM) for genes related to amino acid metabolism was compared with wild type. See Table S1 for list of genes. aaRS production was calibrated in the same way as Figure 1C.

(B) Potential models for aaRS fitness landscape for cells lacking the stringent response. The stringent response may amplify the effects of insufficient tRNA charging (regulation detrimental) or reduce adverse effects (regulation beneficial).

(C) Effects on aaRS fitness landscape of stringent response removal. Strains with stringent response intact (circles) were competed against stringent null cells (squares) across the aaRS production landscape. Measurements of fitness and aaRS production were calculated as in Figure 1. See also Figure S4.

intervals upstream of severely starved codons, suggesting that additional ribosomes are queued behind the waiting ribosome (Figure 5C). This effect is only observed when the stringent response is removed (Figure S5B). Ribosome queuing is potentially a consequence of overcapacity of protein synthesis in strains deficient in the stringent response, which could in turn further exacerbate the growth defect of the cell. In summary, these findings show that RelA-dependent (p)ppGpp synthesis helps avoid adverse effects on translation during forced reduction in tRNA charging.

Importantly, we found that the majority of gene expression changes during aaRS underproduction are mediated through the stringent response. In addition to the translation machinery, the bulk of the changes between wild type and aaRS underproduction involved increased expression of known genes that promote survival under starvation, such as those regulated by CodY and SigB that fail to increase in the stringent null cells (Eymann et al., 2002; Zhang and Haldenwang, 2003) (Figure S5C). Overall, stringent null cells during aaRS underproduction show relatively few expression changes compared with wild type (with intact stringent response and native aaRS levels) (Figure S5C). Of the few increases in expression selectively in the stringent null cells, we find that *clpE*, a AAA+ unfoldase and subunit of the ClpE-ClpP protease, massively increased in expression, indicating potential protein folding stress due to the observed translation pausing. However, despite the few changes and lack of wasteful amino acid biosynthesis expression due to growth in rich media, stringent null cells still display lower fitness. Taken together, we find that the benefits of the coordinated production of translation components outweigh the unnecessary production of amino acid biosynthetic enzymes, making the stringent responsive protective against perturbations in aaRS levels in rich media.

Native Levels of Uncharged tRNAs Cause Limited Stringent Response in Rich Media

If the stringent response remains activated by the native levels of uncharged tRNAs, it could adversely modify the optimal levels aaRS production. However, we found that in the absence of aaRS perturbations, the stringent null cells have similar gene expression patterns as wild-type cells, including ribosomal protein genes, amino acid biosynthetic genes, and CodY-controlled genes (Figure S4C). At the level of translation, eliminating the stringent response with native aaRS production does not lead to substantial differences in ribosome pausing (Figure S5D). These results corroborate the limited fitness effects of the *relA* D264G mutation in otherwise wild-type cells under nutrient-rich conditions (Figure S4B). Further increasing aaRS production from native levels also showed limited differences in (p)ppGpp-regulated genes, ribosome pausing, and fitness (Figures 3D, 4A, S3B, and S4A), which is in stark contrast to aaRS underproduction in the same media. Therefore, the stringent response is sensitively programed to activate with slight aaRS underproduction but not at native levels (Figures 4A and S4A), even though the latter state is also associated with substantial amounts of

Please cite this article in press as: Parker et al., Growth-Optimized Aminoacyl-tRNA Synthetase Levels Prevent Maximal tRNA Charging, Cell Systems (2020), https://doi.org/10.1016/j.cels.2020.07.005

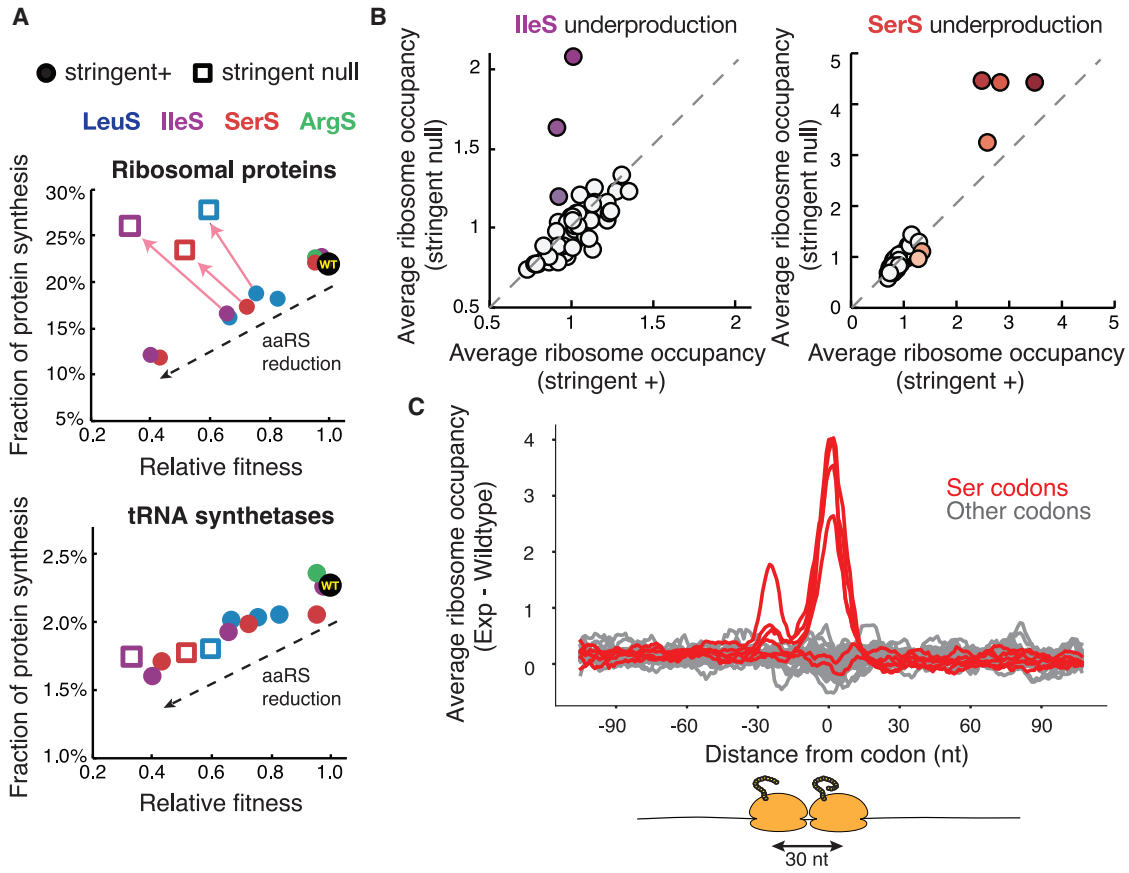

Figure 5. Stoichiometry and Kinetics of Translation Machinery Are Perturbed without Stringent Response

(A) Fraction of protein synthesis devoted to translation-related genes as a function of relative fitness in cells with and without the stringent response. For each inducible aaRS strain at each induction level profiled, the relative fitness as measured by the competition assay was plotted against the fraction of protein synthesis (RPKM) as measured by ribosome profiling for ribosomal proteins and aminoacyl-tRNA synthetases (STAR Methods; Table S1). Stringent positive cells are plotted as closed circles, stringent null cells as open squares. Arrows point to changes when the stringent response is removed at identical induction conditions.

(B) Ribosome occupancy changes due to stringent response removal for IleS and SerS underproduction. Average codon occupancy for 61 sense codons with matched induction conditions is plotted for cells with and without the stringent response. Induction conditions lead to 0.18x and 0.12x native production levels of IleS and SerS based on calibration. Colored codons indicate cognate codons to the inducible aaRS. 310 genes for IleS induction and 218 genes for SerS induction passed the depth threshold in paired experiments and were used for analysis.

(C) Metagene analysis of ribosome pausing and queuing during SerS underproduction in strains lacking the stringent response. Genes were aligned from each of the 61 codons and averaged across them. Difference in ribosome occupancy between SerS underproducing cells without the stringent response and wild type is plotted. Red traces indicate serine codons. For full calculation see STAR Methods. See also Figure S5.

uncharged tRNAs. Taken together, these data show that the stringent response participates in ameliorating the fitness cliff without affecting optimal aaRS production rates.

DISCUSSION

Here, we thoroughly characterized the mechanistic underpinnings of bacterial growth optimization with respect to aminoacyl-tRNA synthetase production. By profiling the molecular and physiological effects that contribute to the overall global fitness landscape, we showed that the production of aaRS proteins is tuned to satisfy the requirement of tRNA charging flux and not to minimize the steady-state levels of uncharged tRNAs during growth in rich media. Moreover, our work yielded insights into several fundamental biological processes that have been well studied in isolation but are nevertheless extensively cross-regulated in living cells.

First, we found that native levels of aaRS production provide limited excess capacity to support translation. For the synthetases examined, a slight decrease from native production rates results in slower translation at cognate codons and a fitness cliff (Figure 6), suggesting that the enzymes are normally operating near saturation in fast growth conditions. This "just enough" aaRS production stands in contrast to the situations of enzymatic overcapacity proposed for other metabolic enzymes, which are thought to be advantageous by providing a buffer against environmental or stochastic fluctuations (Davidi and Milo, 2017; O'Brien et al., 2016; Peters et al., 2016; Sander et al., 2019). Our findings corroborate a recent study on the origin of haploinsufficient genes in yeast suggesting that the

Please cite this article in press as: Parker et al., Growth-Optimized Aminoacyl-tRNA Synthetase Levels Prevent Maximal tRNA Charging, Cell Systems (2020), https://doi.org/10.1016/j.cels.2020.07.005

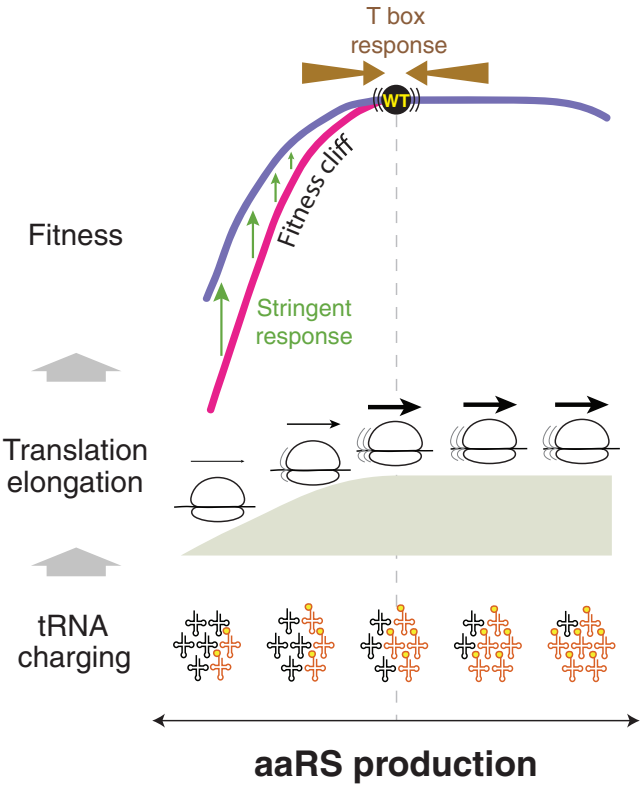

Figure 6. An Integrated View of Growth Optimization for aaRSs

At growth-optimized levels of aaRS production (vertical dashed line), tRNA charging is not yet maximized. However, further increasing aaRS production and tRNA charging does not result in faster translation elongation, leading to no fitness benefit during overproduction. The native levels of aaRS production, with just enough capacity for the amino acid flux into protein synthesis, are positioned near the edge of the fitness cliff in the highly asymmetric landscape. The sharp sensitivity to aaRS underproduction is partially alleviated by the stringent response despite the unnecessary activation of amino acid biosynthesis genes in rich media. Furthermore, the T box-based autoregulation buffers perturbations to aaRS production from both directions, which is enabled by having non-maximized tRNA charging at the native levels.

expression of haploinsufficient genes are limited by fitness costs associated with their overexpression (Morrill and Amon, 2019). In the case of aaRSs, we found that even a small fitness defect of overproduction, by comparison with underproduction, could drive evolution toward an expression that is next to the fitness cliff. In addition, the homeostatic feedback of uncharged tRNAs on aaRS production may further ensure that cells maintain sufficient tRNA charging capacity for translation elongation (Figure 6). Whether or not these same principles apply to growth in nutrient-poor conditions when amino acids must be synthesized *de novo* remains to be explored. Finally, given that all four aaRSs tested here show limited excess capacity, our findings demonstrate that bacterial growth may be limited simultaneously by multiple enzymes in the terms of their underproduction and not overproduction, akin to ribosomal production.

Second, our results show that the feedback regulation for aaRS synthesis is programed to prevent both overproduction and underproduction despite the highly asymmetric fitness landscape (Figure 6). As a homeostatic mechanism, negative feedback regulation may not be constantly active. In one design scenario, the feedback may be constitutively on and inactivated only during reduced output to ensure sufficient charging capacity. Alternatively, it may be constitutively off and activated only during excessive output to prevent wasteful aaRS production. Although the extreme sensitivity to aaRS underproduction suggests a priority to ensure sufficient charging capacity, our T box reporters show that the native autoregulation remains responsive to both under and overproduction, which is consistent with a previous report for *thrS* and *valS* (Gendron et al., 1994; Luo et al., 1997). Therefore, the negative feedback loop for aaRS has not evolved to be a merely single-purpose device that is protective in only one direction. Importantly, this ability to respond in both regimes is rooted in the fact that the signal for feedback, i.e., tRNA charging, is not fully saturated at the native aaRS production (Figure 6).

Finally, similar to how translation speed is only sensitive to aaRS underproduction, global growth regulation by the stringent response is activated with mild aaRS reduction while having limited effects at native uncharged tRNA levels. Although it is possible that some (p)ppGpp is produced with native aaRS production or even in the *relA* D264G mutant used here, our gene expression data for aaRS overproduction suggest that these basal uncharged tRNA levels do not substantially activate the stringent response. Given that the native uncharged fraction is estimated to be 10%–50% for most tRNAs, the concentration of uncharged tRNAs cannot increase drastically with a small decrease in aaRS production. How the stringent response is programed to be sharply activated by small changes in uncharged tRNA levels remains to be resolved, and recent structural analyses on how RelA is activated on the ribosome may provide insights (Loveland et al., 2016; Winther et al., 2018). Upon activation, the stringent response curbs ribosome biogenesis and promotes *de novo* amino acid biosynthesis. However, the latter likely leads to wasteful production of anabolic enzymes when aaRS is limiting in the presence of externally supplied amino acids. It is, therefore, striking that we observed a strong protective effect of the stringent response during aaRS limitation (Figure 6). We propose that the maintenance of protein stoichiometry for the translation apparatus contributes to the protective effect. Without the stringent response, ribosomal protein and some translation factors remain highly expressed, whereas most aaRSs (in addition to the limiting one) have reduced expression in line with the growth rate. The resulting imbalance between ribosomes and aaRSs, together with defects in other (p)ppGpp-dependent regulation (Srivatsan and Wang, 2008; Trinquier et al., 2019), may lead to the observed translation defects, including exacerbated ribosome pausing and queuing. This result underscores the importance of proper stoichiometry among functionally associated proteins and offers an explanation for the broadly conserved protein stoichiometry across a wide range of species (Lalanne et al., 2018).

Elucidating the interdependence between gene expression, protein activities, and cellular fitness is a fundamental problem in systems biology. With the rapidly expanding knowledge of gene expression and protein functions, a key challenge is to understand how these molecular properties are integrated *in vivo* to define the behavior of a cell. Our work outlines an approach to

connect the fitness landscape to its mechanistic understandings, providing powerful insight into the optimization of protein abundance and regulation.

STAR★METHODS

Detailed methods are provided in the online version of this paper and include the following:

- KEY RESOURCES TABLE
- RESOURCE AVAILABILITY
  - Lead Contact
  - Materials Availability
  - Data and Code Availability
- EXPERIMENTAL MODEL AND SUBJECT DETAILS
  - Strain Construction
- METHOD DETAILS
  - Strain Construction
  - Growth Media
  - qRT-PCR
  - Ribosome Profiling
  - RNA Sequencing
  - AUPAGE & Northern Blot
  - Competition Experiments
- QUANTIFICATION AND STATISTICAL ANALYSIS
  - Fitness Calculation
  - Calibration of aaRS Production
  - Ribosome Profiling and RNA-seq Data Analysis

SUPPLEMENTAL INFORMATION

Supplemental Information can be found online at https://doi.org/10.1016/j.cels.2020.07.005.

ACKNOWLEDGMENTS

We thank members of the MIT BioMicro Center for help in design and completion of the high-throughput sequencing; members of the Li lab and Grossman lab for discussions. This research is supported by NIH R35GM124732, Pew Biomedical Scholars Program, a Sloan Research Fellowship, Searle Scholars Program, the Smith Family Award for Excellence in Biomedical Research, an NIH Pre-Doctoral training grant (T32 GM007287, to D.J.P. and G.E.J.), an NSF graduate research fellowship (to G.E.J.), an NSERC graduate fellowship (Canada, to J.B.L.), and an HHMI International Student Fellowship (to J.B.L.). S.K.'s work in the laboratory of M.K.W. is supported by the HHMI and NIH grant R01-AI-042347.

AUTHOR CONTRIBUTIONS

D.J.P. and G.-W.L. designed the experiments and analysis. J.B.L. and D.J.P. designed and optimized the competition experiment. D.J.P. and S.K. performed the tRNA charging experiments. D.J.P. and G.E.J. created the strains for the experiments. D.J.P. and G.-W.L. wrote the manuscript. S.K., M.K.W., and J.B.L. edited the manuscript.

DECLARATION OF INTERESTS

The authors declare no competing interests.

Received: December 22, 2019
Revised: May 7, 2020
Accepted: July 2, 2020
Published: July 28, 2020

REFERENCES

Avcilar-Kucukgoze, I., Bartholomäus, A., Cordero Varela, J.A., Kaml, R.F.-X., Neubauer, P., Budisa, N., and Ignatova, Z. (2016). Discharging tRNAs: a tug of war between translation and detoxification in Escherichia coli. Nucleic Acids Res. *44*, 8324–8334.

Bremer, H., and Dennis, P.P. (2008). Modulation of chemical composition and other parameters of the cell at different exponential growth rates. EcoSal Plus *3*, https://doi.org/10.1128/ecosal.5.2.3.

Britton, R.A., Eichenberger, P., Gonzalez-Pastor, J.E., Fawcett, P., Monson, R., Losick, R., and Grossman, A.D. (2002). Genome-wide analysis of the stationary-phase sigma factor (sigma-H) regulon of Bacillus subtilis. J. Bacteriol. *184*, 4881–4890.

Dai, X., Zhu, M., Warren, M., Balakrishnan, R., Patsalo, V., Okano, H., Williamson, J.R., Fredrick, K., Wang, Y.-P., and Hwa, T. (2016). Reduction of translating ribosomes enables Escherichia coli to maintain elongation rates during slow growth. Nat. Microbiol. *2*, 16231.

Darnell, A.M., Subramaniam, A.R., and O'Shea, E.K. (2018). Translational control through differential ribosome pausing during amino acid limitation in mammalian cells. Mol. Cell *71*, 229–243.e11.

Davidi, D., and Milo, R. (2017). Lessons on enzyme kinetics from quantitative proteomics. Curr. Opin. Biotechnol. *46*, 81–89.

Dekel, E., and Alon, U. (2005). Optimality and evolutionary tuning of the expression level of a protein. Nature *436*, 588–592.

Dittmar, K.A., Mobley, E.M., Radek, A.J., and Pan, T. (2004). Exploring the regulation of tRNA distribution on the genomic scale. J. Mol. Biol. *337*, 31–47.

Dittmar, K.A., Sørensen, M.A., Elf, J., Ehrenberg, M., and Pan, T. (2005). Selective charging of tRNA isoacceptors induced by amino-acid starvation. EMBO Rep *6*, 151–157.

Dong, H., Nilsson, L., and Kurland, C.G. (1995). Gratuitous overexpression of genes in Escherichia coli leads to growth inhibition and ribosome destruction. J. Bacteriol. *177*, 1497–1504.

Elf, J., Nilsson, D., Tenson, T., and Ehrenberg, M. (2003). Selective charging of tRNA isoacceptors explains patterns of codon usage. Science *300*, 1718–1722.

Eymann, C., Homuth, G., Scharf, C., and Hecker, M. (2002). Bacillus subtilis functional genomics: global characterization of the stringent response by proteome and transcriptome analysis. J. Bacteriol. *184*, 2500–2520.

Ferro, I., Liebeton, K., and Ignatova, Z. (2017). Growth-rate dependent regulation of tRNA level and charging in Bacillus licheniformis. J. Mol. Biol. *429*, 3102–3112.

Gendron, N., Putzer, H., and Grunberg-Manago, M. (1994). Expression of both Bacillus subtilis threonyl-tRNA synthetase genes is autogenously regulated. J. Bacteriol. *176*, 486–494.

Gibson, D.G., Young, L., Chuang, R.Y., Venter, J.C., Hutchison, C.A., and Smith, H.O. (2009). Enzymatic assembly of DNA molecules up to several hundred kilobases. Nat. Methods *6*, 343–345.

Giegé, R., and Springer, M. (2016). Aminoacyl-tRNA synthetases in the bacterial world. EcoSal Plus *7*, https://doi.org/10.1128/ecosalplus.ESP-0002-2016.

Gloge, F., Becker, A.H., Kramer, G., and Bukau, B. (2014). Co-translational mechanisms of protein maturation. Curr. Opin. Struct. Biol. *24*, 24–33.

Gourse, R.L., Chen, A.Y., Gopalkrishnan, S., Sanchez-Vazquez, P., Myers, A., and Ross, W. (2018). Transcriptional responses to ppGpp and DksA. Annu. Rev. Microbiol. *72*, 163–184.

Gouy, M., and Grantham, R. (1980). Polypeptide elongation and tRNA cycling in Escherichia coli: a dynamic approach. FEBS Lett *115*, 151–155.

Green, N.J., Grundy, F.J., and Henkin, T.M. (2010). The T box mechanism: tRNA as a regulatory molecule. FEBS Lett *584*, 318–324.

Gutiérrez-Preciado, A., Henkin, T.M., Grundy, F.J., Yanofsky, C., and Merino, E. (2009). Biochemical features and functional implications of the RNA-based T-box regulatory mechanism. Microbiol. Mol. Biol. Rev. *73*, 36–61.

Hanson, G., and Coller, J. (2018). Codon optimality, bias and usage in translation and mRNA decay. Nat. Rev. Mol. Cell Biol. *19*, 20–30.

Hauryliuk, V., Atkinson, G.C., Murakami, K.S., Tenson, T., and Gerdes, K. (2015). Recent functional insights into the role of (p)ppGpp in bacterial physiology. Nat. Rev. Microbiol. *13*, 298–309.

Hinnebusch, A.G. (2005). Translational regulation of GCN4 and the general amino acid control of yeast. Annu. Rev. Microbiol. *59*, 407–450.

Kimura, S., and Waldor, M.K. (2019). The RNA degradosome promotes tRNA quality control through clearance of hypomodified tRNA. Proc. Natl. Acad. Sci. USA *116*, 1394–1403.

Klumpp, S., Scott, M., Pedersen, S., and Hwa, T. (2013). Molecular crowding limits translation and cell growth. Proc. Natl. Acad. Sci. USA *110*, 16754–16759.

Klumpp, S., Zhang, Z., and Hwa, T. (2009). Growth rate-dependent global effects on gene expression in bacteria. Cell *139*, 1366–1375.

Kriel, A., Brinsmade, S.R., Tse, J.L., Tehranchi, A.K., Bittner, A.N., Sonenshein, A.L., and Wang, J.D. (2014). GTP dysregulation in Bacillus subtilis cells lacking (p)ppGpp results in phenotypic amino acid auxotrophy and failure to adapt to nutrient downshift and regulate biosynthesis genes. J. Bacteriol. *196*, 189–201.

Lalanne, J.B., Taggart, J.C., Guo, M.S., Herzel, L., Schieler, A., and Li, G.W. (2018). Evolutionary convergence of pathway-specific enzyme expression stoichiometry. Cell *173*, 749–761.e38.

Langmead, B., Trapnell, C., Pop, M., and Salzberg, S.L. (2009). Ultrafast and memory-efficient alignment of short DNA sequences to the human genome. Genome Biol *10*, R25.

Li, G.-W., Burkhardt, D., Gross, C., and Weissman, J.S. (2014). Quantifying absolute protein synthesis rates reveals principles underlying allocation of cellular resources. Cell *157*, 624–635.

Liang, S., Bipatnath, M., Xu, Y., Chen, S., Dennis, P., Ehrenberg, M., and Bremer, H. (1999). Activities of constitutive promoters in Escherichia coli. J. Mol. Biol. *292*, 19–37.

Liu, K., Bittner, A.N., and Wang, J.D. (2015). Diversity in (p)ppGpp metabolism and effectors. Curr. Opin. Microbiol. *24*, 72–79.

Loveland, A.B., Bah, E., Madireddy, R., Zhang, Y., Brilot, A.F., Grigorieff, N., and Korostelev, A.A. (2016). Ribosome•RelA structures reveal the mechanism of stringent response activation. eLife *5*, 811.

Luo, D., Leautey, J., Grunberg-Manago, M., and Putzer, H. (1997). Structure and regulation of expression of the Bacillus subtilis valyl-tRNA synthetase gene. J. Bacteriol. *179*, 2472–2478.

McClain, W.H., Jou, Y.Y., Bhattacharya, S., Gabriel, K., and Schneider, J. (1999). The reliability of in vivo structure-function analysis of tRNA aminoacylation. J. Mol. Biol. *290*, 391–409.

Morrill, S.A., and Amon, A. (2019). Why haploinsufficiency persists. Proc. Natl. Acad. Sci. USA *116*, 11866–11871.

Nanamiya, H., Kasai, K., Nozawa, A., Yun, C.S., Narisawa, T., Murakami, K., Natori, Y., Kawamura, F., and Tozawa, Y. (2008). Identification and functional analysis of novel (p)ppGpp synthetase genes in Bacillus subtilis. Mol. Microbiol. *67*, 291–304.

O'Brien, E.J., Utrilla, J., and Palsson, B.O. (2016). Quantification and classification of E. coli proteome utilization and unused protein costs across environments. PLoS Comput. Biol. *12*, e1004998.

Peters, J.M., Colavin, A., Shi, H., Czarny, T.L., Larson, M.H., Wong, S., Hawkins, J.S., Lu, C.H.S., Koo, B.M., Marta, E., et al. (2016). A comprehensive, CRISPR-based functional analysis of essential genes in bacteria. Cell *165*, 1493–1506.

Potrykus, K., and Cashel, M. (2008). (p)ppGpp: still magical? Annu. Rev. Microbiol. *62*, 35–51.

Putzer, H., Laalami, S., Brakhage, A.A., Condon, C., and Grunberg-Manago, M. (1995). Aminoacyl-tRNA synthetase gene regulation in Bacillus subtilis: induction, repression and growth-rate regulation. Mol. Microbiol. *16*, 709–718.

Rauscher, R., and Ignatova, Z. (2018). Timing during translation matters: synonymous mutations in human pathologies influence protein folding and function. Biochem. Soc. Trans. *46*, 937–944.

Sander, T., Farke, N., Diehl, C., Kuntz, M., Glatter, T., and Link, H. (2019). Allosteric feedback inhibition enables robust amino acid biosynthesis in E. coli by enforcing enzyme overabundance. Cell Syst *8*, 66–75.e8.

Schneider, C.A., Rasband, W.S., and Eliceiri, K.W. (2012). NIH Image to ImageJ: 25 years of image analysis. Nat. Methods *9*, 671–675.

Scott, M., Gunderson, C.W., Mateescu, E.M., Zhang, Z., and Hwa, T. (2010). Interdependence of cell growth and gene expression: origins and consequences. Science *330*, 1099–1102.

Scott, M., and Hwa, T. (2011). Bacterial growth laws and their applications. Curr. Opin. Biotechnol. *22*, 559–565.

Sherman, J.M., Rogers, M.J., and Söll, D. (1992). Competition of aminoacyl-tRNA synthetases for tRNA ensures the accuracy of aminoacylation. Nucleic Acids Res *20*, 2847–2852.

Sonenshein, A.L. (2005). CodY, a global regulator of stationary phase and virulence in Gram-positive bacteria. Curr. Opin. Microbiol. *8*, 203–207.

Srivatsan, A., and Wang, J.D. (2008). Control of bacterial transcription, translation and replication by (p)ppGpp. Curr. Opin. Microbiol. *11*, 100–105.

Stead, M.B., Agrawal, A., Bowden, K.E., Nasir, R., Mohanty, B.K., Meagher, R.B., and Kushner, S.R. (2012). RNAsnap™: a rapid, quantitative and inexpensive, method for isolating total RNA from bacteria. Nucleic Acids Res *40*, e156.

Subramaniam, A.R., Deloughery, A., Bradshaw, N., Chen, Y., O'Shea, E., Losick, R., and Chai, Y. (2013a). A serine sensor for multicellularity in a bacterium. eLife *2*, e01501.

Subramaniam, A.R., Pan, T., and Cluzel, P. (2013b). Environmental perturbations lift the degeneracy of the genetic code to regulate protein levels in bacteria. Proc. Natl. Acad. Sci. USA *110*, 2419–2424.

Subramaniam, A.R., Zid, B.M., and O'Shea, E.K. (2014). An integrated approach reveals regulatory controls on bacterial translation elongation. Cell *159*, 1200–1211.

Swanson, R., Hoben, P., Sumner-Smith, M., Uemura, H., Watson, L., and Söll, D. (1988). Accuracy of in vivo aminoacylation requires proper balance of tRNA and aminoacyl-tRNA synthetase. Science *242*, 1548–1551.

Tockman, J., and Vold, B.S. (1977). In vivo aminoacylation of transfer ribonucleic acid in Bacillus subtilis and evidence for differential utilization of lysine-isoaccepting transfer ribonucleic acid species. J. Bacteriol. *130*, 1091–1097.

Trinquier, A., Ulmer, J.E., Gilet, L., Figaro, S., Hammann, P., Kühn, L., Braun, F., and Condon, C. (2019). tRNA maturation defects lead to inhibition of rRNA processing via synthesis of pppGpp. Mol. Cell *74*, 1227–1238.e3.

Varshney, U., Lee, C.P., and RajBhandary, U.L. (1991). Direct analysis of aminoacylation levels of tRNAs in vivo. Application to studying recognition of Escherichia coli initiator tRNA mutants by glutaminyl-tRNA synthetase. J. Biol. Chem. *266*, 24712–24718.

Vitreschak, A.G., Mironov, A.A., Lyubetsky, V.A., and Gelfand, M.S. (2008). Comparative genomic analysis of T-box regulatory systems in bacteria. Rna *14*, 717–735.

Winther, K.S., Roghanian, M., and Gerdes, K. (2018). Activation of the stringent response by loading of RelA-tRNA complexes at the ribosomal A-site. Mol. Cell *70*, 95–105.e4.

Wu, C.C.-C., Zinshteyn, B., Wehner, K.A., and Green, R. (2019). High-resolution ribosome profiling defines discrete ribosome elongation states and translational regulation during cellular stress. Mol. Cell *73*, 959–970.e5.

Yegian, C.D., Stent, G.S., and Martin, E.M. (1966). Intracellular condition of Escherichia coli transfer RNA. Proc. Natl. Acad. Sci. USA *55*, 839–846.

Zhang, S., and Haldenwang, W.G. (2003). RelA is a component of the nutritional stress activation pathway of the Bacillus subtilis transcription factor sigma B. J. Bacteriol. *185*, 5714–5721.

Zhu, M., and Dai, X. (2019). Growth suppression by altered (p)ppGpp levels results from non-optimal resource allocation in Escherichia coli. Nucleic Acids Res *47*, 4684–4693.

Please cite this article in press as: Parker et al., Growth-Optimized Aminoacyl-tRNA Synthetase Levels Prevent Maximal tRNA Charging, Cell Systems (2020), https://doi.org/10.1016/j.cels.2020.07.005

STAR★METHODS

KEY RESOURCES TABLE

REAGENT or RESOURCE	SOURCE	IDENTIFIER
Bacterial and Virus Strains		
Bacillus subtilis strains	This Paper	See Table S5
Chemicals, Peptides, and Recombinant Proteins		
Chemicals for MCCG Media	This Study	See Table S3
Trichloroacetic Acid	Sigma	T6399
Isopropanol	Macron	3032-16
1M Tris pH 9.5	Teknova	T1095
Qubit BR RNA	ThermoFisher	Q10210
Superase-IN RNase	ThermoFisher	AM2696
PerfectHyb Plus Hybridization buffer	Sigma	H7033
Glycoblue	ThermoFisher	AM9516
Corning® 500 mL 0.2 μm Pore filter	Corning	430773
Select-a-size DNA Clean & Concentrator	Zymo	D4080
NEBuilder HiFi DNA Assembly Master Mix	New England Biolabs	E2621S
DNase I recombinant, RNase-free (Roche)	Sigma-Aldrich	4716728001
Micrococcal nuclease	Roche	No longer available
T4 Polynucleotide Kinase (PNK)	New England Biolabs	M0201S
SuperScript III Reverse Transcriptase	ThermoFisher Scientific	18080093
CircLigase ssDNA ligase	Lucigen	CL4115K
Dynabeads MyOne Streptavidin C1	ThermoFisher Scientific	65001
Q5 High-Fidelity DNA Polymerase	New England Biolabs	M0491L
T4 RNA ligase 2 truncated K277Q	J. Weissman	N/A
ATP, [γ-^{32}P]	PerkinElmer	BLU502A250UC
SuperScript III Reverse Transcriptase	Thermo Fisher Scientific	18080044
G25 Sepharose columns	GE Healthcare Life Sciences	27532501
Critical Commercial Assays		
RNeasy Mini kit	QIAGEN	74104
MICROBExpress Bacterial mRNA Enrichment Kit	ThermoFisher Scientific	AM190
Oligo Clean & Concentrator	Zymo Research	D4060
Deposited Data		
Raw .fastq and processed .wig files from Ribosome profiling	This paper	GEO: GSE141389
Northern blots raw data	This paper; Mendeley data	https://doi.org/10.17632/f9kkszrtch.1
Experimental Models: Organisms/Strains		
Bacillus subtilis strains	This Paper	See Table S5
Oligonucleotides		
Northern Blot assay probes	This paper	See Table S2
RT-qPCR primers	This paper	See Table S2
Library preparation primers	This paper	See Table S2
Strain creation primers	This paper	See Table S2
Competition experiment primers	This paper	See Table S2
Software and Algorithms		
Bowtie v2.0.0b3	Langmead et al., 2009	http://bowtie-bio.sourceforge.net/index.shtml
Python 2.7	Python Software Foundation	http://www.python.org

(*Continued on next page*)

Please cite this article in press as: Parker et al., Growth-Optimized Aminoacyl-tRNA Synthetase Levels Prevent Maximal tRNA Charging, Cell Systems (2020), https://doi.org/10.1016/j.cels.2020.07.005

Continued

REAGENT or RESOURCE	SOURCE	IDENTIFIER
Other custom python scripts	This paper	Available upon request
ImageJ	Schneider et al., 2012	https://imagej.nih.gov/ij/
Other		
Super Membrane Disc Filters, Pall Laboratory	VWR	28147-980
Grinding Jar Set, Stainless Steel	Qiagen	69985
TissueLyser II	Qiagen	85300
Novex TBE-Urea gels, 15%	ThermoFisher	EC6885BOX
Novex TBE-Urea gels, 10%	ThermoFisher	EC6875BOX
Novex TBE gels, 8%	ThermoFisher	EC62152BOX

RESOURCE AVAILABILITY

Lead Contact

Further information and request for resources and reagents should be directed to and will be fulfilled by the Lead Contact, Gene-Wei Li (gwli@mit.edu).

Materials Availability

This study did not generate new unique reagents.

Data and Code Availability

The Ribosome profiling and RNA sequencing datasets generated during this study are available at the Gene Expression Omnibus with accession number GSE141389. The raw sequencing files of the amplicons generated from competition experiments is available in the NCBI Sequencing Read Archive (SRA) under accession number PRJNA593245. Full code is available upon request. The raw image for Northern blots was deposited at Mendeley Data and can be viewed at http://dx.doi.org/10.17632/f9kkszrtch.1.

EXPERIMENTAL MODEL AND SUBJECT DETAILS

Strain Construction

Bacillus subtilis 168 strain was used as the wild-type strain and base strain for transformations. All further strains were constructed using natural competence as described below. For all assays, cells were grown in a defined rich minimal media (MCCG) described below. All inducible aaRS strains were created by first cloning individual aaRS ORFs under the PspankHY promoter system in a plasmid containing the *lac* repressor, a spectinomycin resistance cassette, and flanked by 500 nt homology arms of the *amyE* locus (Britton et al., 2002). After creation, plasmids were linearized, transformed into *B. subtilis* 168, and selected with 100 μg/mL spectinomycin. To remove the native copy of the aaRS gene, a transcriptional fusion of GFP and a chloramphenicol resistance cassette (CmR) was assembled using Gibson assembly with additional flanking 500-nucleotide homology arms to the aaRS locus of interest (Gibson et al., 2009). The complete linearized DNA product were directly transformed into the inducible aaRS strains and selected on LB-agar plates with 5 μg/mL chloramphenicol and 100 μM IPTG. To the generate stringent null strains, a gBlock DNA fragment (Integrated DNA technologies) was purchased containing 378 nt of the *relA* gene sequence: 186 nt upstream and 189 nt downstream of codon 264 while changing codon 264 GAT (Asp) to GGT (Gly). The full sequence can be found in Table S2. Fragments containing further upstream and downstream arms of the *relA* locus as well as a Kanamycin resistance gene (KanR) were assembled. Upon full product amplification by PCR, DNA was transformed into strains and selected on LB plates with 10 μg/mL Kanamycin.

METHOD DETAILS

Strain Construction

Competent cells were prepared by following protocol; Cells to be transformed were streaked onto LB plates with the appropriate selection marker. The following morning a single colony was picked into 5 mL of LM media (LB + 3 mM MgSO4). Cultures were incubated at 37°C with shaking until OD_{600} was between 0.8 and 1.2. 300 μL of cells were then transferred to 3 mL competence media (1% Glucose, 3 mM MgSO4, 2.5 mg/mL Potassium Aspartate, 11 μg/mL Ferric Ammonium Citrate, 40 μg/mL Tryptophan, 10.7 g/L Dipotassium Phosphate, 6 g/L Monopotassium Phosphate, 1 g/L Trisodium Citrate Dihydrate) and incubated with shaking for 3.5 h at 37°C. A 200 μL aliquot of competent cells was mixed with 100-1000 ng of DNA and shaken at 37°C for an additional 1.5 h before plating on the appropriate selection plates. Selection was performed on LB agar plates using the following concentrations of antibiotics; 10 μg /mL Kanamycin, 100 ng/mL Spectinomycin, 5 μg /mL Chloramphenicol, and/or 10 μg/mL Tetracycline.

Please cite this article in press as: Parker et al., Growth-Optimized Aminoacyl-tRNA Synthetase Levels Prevent Maximal tRNA Charging, Cell Systems (2020), https://doi.org/10.1016/j.cels.2020.07.005

Growth Media

For all experiments, a defined rich media was used for growth of cells (MCCG). See Table S3 for a complete recipe. Given the essentiality of the aaRS genes tested, all strain maintenance, overnight growth conditions, or LB-agar plates included 100 μM IPTG. For competition experiments "conditioned MCCG" media was used instead of fresh MCCG media. To create conditioned MCCG, wildtype *B. subtilis* 168 was back-diluted 2000-fold from an overnight culture into 0.5 L of fresh MCCG media. Cells were grown with vigorous shaking at 37°C until OD_{600} = 0.2. The culture was then immediately poured over a 0.2 μm vacuum filtration flask, collecting the sterilized "conditioned" MCCG media. We found that conditioned MCCG media nearly eliminates a lag phase (0–5 min) upon back-dilution during the competition experiment while fresh MCCG induces a 10–15 minute lag phase before the resumption of exponential growth (data not shown).

qRT-PCR

For qRT-PCR measurements, overnight cultures of cells were back-diluted 1000-fold and grown in fresh MCCG media with the appropriate concentration of IPTG. When the culture reached OD_{600} = 0.3, cells were collected by mixing 5 mL of culture with 5 mL of ice-cold methanol. After 10 min on ice, cells were spun down at 4°C for 10 min, decanted of excess liquid and resuspended in 100 μL of a solution containing 10 mg/mL Lysozyme, 10 mM Tris-HCl pH 7, and 1 mM EDTA. RNA was extracted using RNeasy Mini Kits (Qiagen) according to the manufacturers protocols for Gram-positive Bacteria. Random hexamer reverse transcription with Moloney Murine Leukemia Virus (M-MuLV) (M0253; NEB) was performed according to the manufacturer's specifications. Gene expression changes were normalized to *sigA*. For a list of primers used see Table S2.

Ribosome Profiling

For ribosome profiling experiments, cells were grown in fresh MCCG media, using a protocol outlined previously (Lalanne et al., 2018; Li et al., 2014). An overnight liquid culture, started from a single colony from a fresh plate, was diluted about 5,000-fold into 250 mL fresh MCCG media in a 2.8 L flask at 37°C with aeration (200 rpm) until OD_{600} = 0.4. The cell culture was rapidly filtered over a nitrocellulose filter and scraped into liquid nitrogen at 37°C. Cell pellets were combined with 650 mL of frozen droplets of lysis buffer 10 mM MgCl2 , 100 mM NH4 Cl, 20 mM Tris pH 8.0, 0.1% NP-40, 0.4% Triton X-100, 100 U/mL DNase I, and 1 mM chloramphenicol. Cells and lysis buffer were pulverized in 10 mL canisters prechilled in liquid nitrogen using a TissueLyser II (Qiagen) for 5 cycles of 3 min at 15 Hz. Pulverized lysate was thawed on ice and clarified by centrifugation at 20,000 rcf. for 10 min at 4°C. 0.5 mg of clarified lysate was then digested with 5 mM CaCl2 and 750 U of micrococcal nuclease (Roche) at 25°C for 1 hr before quenching with 6 mM EGTA.

Following nuclease digestion, the monosome fraction was collected using sucrose gradient and the RNA extracted by hot-phenol extraction. Ribosome-protected mRNA fragments (footprints) with size ranging from 15 to 45 nucleotides were size selected on a polyacrylamide gel. Footprint RNA was dephosphorylated using T4 polynucleotide kinase (NEB) at 37°C for 1 h. Three picomoles of footprints were ligated to 100 pmole of 5' adenylated and 3' end blocked DNA oligo (Linker-1, Table S2) using truncated T4 RNA ligase 2 K277Q at 37°C for 2.5 hr. The ligated product was purified by using polyacrylamide gel. cDNA was generated using Superscript III (Thermo Fisher) and custom primer oCJ485 (Table S2) and isolated by size excision on a polyacrylamide gel.

Single-stranded cDNA was circularized using 100 U of CircLigase (Lucigen) at 60°C for 2 hr. Ribosomal cDNA fragments were removed using biotin-linked custom DNA oligos (Table S2) and MyOne Streptavidin C1 Dynabeads (Thermo Fisher). Final cDNA was amplified using Q5 DNA polymerase (NEB) with o231 primer and indexing primers (Table S2). Sequencing was performed on an Illumina HiSeq 2000 or NextSeq500.

RNA Sequencing

For RNA-seq experiments, overnight cultures of cells were back-diluted 1000-fold and grown in fresh MCCG media with the appropriate concentration of IPTG. When the culture reached OD_{600} = 0.3, cells were collected by mixing 9 mL of culture with 1 mL of ice-cold stop solution (95% Ethanol, 5% Phenol). Cells were spun down for 10 min at 20,000 rcf in a 4°C centrifuge. Excess solution was decanted and removed by pipette. Cell pellets were resuspended in 200 μL 10mM Tris-HCL 1mM EDTA and split into two 100-μL fractions.

To one fraction, cells were lysed with 10 mg/mL lysozyme and RNA extracted using RNeasy column (*Qiagen #74104*). Purified RNA was ribosomal RNA depleted with MICROBExpress Bacterial mRNA Enrichment Kit (*ThermoFischer #AM1905*) according to the manufacturer's instructions. RNA from these samples was to be used for gene expression experiments having been depleted for rRNA and tRNA.

To the other fraction, the 100 μL aliquot was re-spun and liquid was removed by pipette. RNA from cell pellet was extracted using RNASnap (Stead et al., 2012). Briefly, cell pellets were resuspended in 500 μL Extraction solution (95% Formamide, 1% BME, 0.025% SDS, 18 mM EDTA) and 200 μL chilled zirconia beads (0.1 mm diameter). Resuspensions were vortexed for 10 min using a horizontal vortex adapter, incubated for 7 min at 95°C, and 300 μL of the aqueous solution was transferred to a fresh tube. Samples were spun for 5 min at 16,000g and supernatant was diluted with four volumes of water in a fresh tube and precipitated with five volumes of Isopropanol. After freezing and centrifugation, RNA was resuspended in 10 mM Tris pH 7. RNA from these samples was to be used for total RNA expression experiments and was not depleted for rRNA or tRNA.

Please cite this article in press as: Parker et al., Growth-Optimized Aminoacyl-tRNA Synthetase Levels Prevent Maximal tRNA Charging, Cell Systems (2020), https://doi.org/10.1016/j.cels.2020.07.005

Each RNA sample was then fragmented (*ThermoFischer #AM8740*), dephosphorylated, polyadenlyated, and reverse transcribed using Superscript III and custom oligo-dT reverse transcription primers. Resulting cDNA was ligated with Illumina sequencing adapters and PCR amplified+. Single end (50 bp) sequencing was performed on an Illumina NextSeq.

AUPAGE & Northern Blot

tRNA charging analysis was performed similarly to (Darnell et al., 2018; Kimura and Waldor, 2019; Varshney et al., 1991). Cells were grown to OD_{600} 0.3, mixed 50:50 with pre-warmed 10% Trichloroacetic Acid, and placed on ice. Mixtures were spun down at 3000 x g for 10 min at 4°C and the supernatant was poured off. Cell pellets were then resuspended in 750 μL of AE buffer (0.3 M NaOAc pH 4.5, 10 mM EDTA) and either frozen at -80°C or immediately mixed with 750 μL ice cold Phenol pH 4.5 before transferring to a 2 mL tube. Mixtures were vortexed for 10 min, rested on ice for 5 min, and spun for 10 min at 4°C. Aqueous supernatant was removed and mixed with 750 μL cold Isopropanol. Another 750 μL of AE buffer was then added to the remaining organic layer before another round of vortexing and separation was performed. The aqueous layer was transferred to another tube with 750 μL cold Isopropanol and all samples were vortexed and precipitated for more than 2 h at -20°C. After spinning down precipitations, pellets were washed with 70:30::Ethanol:10 mM NaOAc pH 4.5 and dried. Pellets were re-dissolved in SA Buffer (10 mM NaOAc pH 4.5, 1 mM EDTA) and quantified using Qubit BR RNA kit. To mark gel mobility shift of uncharged tRNA, total RNA samples were deacylated in 100 mM Tris pH 9.5 at 37° for 1 h then precipitated and re-dissolved in SA buffer.

To perform the acid urea gel electrophoresis, 0.5 – 1 μg of each sample was mixed with 2X loading buffer (0.1 M NaOAc pH 5.0, 9 M urea, 0.05% bromophenol blue, and 0.05% xylene cyanol) and loaded onto a gel containing 6.5% polyacrylamide, 7 M Urea, and 0.1 M NaOAc pH 5.0. Following electrophoresis, the region between the bromophenol blue and xylene cyanol bands was excised and washed in 1X TBE. Gels were transferred to BrightStar-Plus positively charged nylon membrane in 1X TBE using a semi-dry transfer apparatus at 3 mA/cm^2 for 30 min. The blots were crosslinked twice with 1,200 μJ UV light, prehybridized in PerfectHyb buffer for 30 min at 42°C, and hybridized at 42°C with 5 pmol of the appropriate probe (see Table S2). Probes were end-labeled with [γ-32P] ATP using T4 PNK and purified with G25 Sepharose columns. Blots were twice washed with Wash Buffer (2X SSC and 0.5% SDS) at 60°C, exposed to a Phosphor-Imaging screen for 1 h, and imaged using a FLA-5000 phosphoimager (Fuji). To properly assess the absolute charging level for samples with very high charging fractions, we first extracted raw intensities from the northern blot using ImageJ (Schneider et al., 2012). Using the x-coordinates of positions of maximal peak heights in wildtype lanes, we fit two gaussians around the uncharged and charged fractions and calculated the area under the curve. The charged fraction was calculated as the area under the charged band divided by the sum of the charged and uncharged bands. These peak positions were used to fit curves for both bands in the aaRS overproduction samples, calculating the charging ratio in the same way.

Competition Experiments

To barcode strains for competition analysis a bar-coding plasmid was created to integrate at the *lacA* locus with a tetracycline resistance gene *tetM* (genotype *lacA::BC-tetM*). Each plasmid has a random 12 nucleotide sequence near the end of *lacA* integration site to replace the endogenous sequence and differentiate the strain from the others by DNA sequence. All "strain-types" (i.e. *argS* inducible strain or *ileS* inducible with *relA* D254G mutation strain) used in the competition experiment except for wildtype 168 were transformed with the barcoding plasmid. For all strain-types used in the experiment, 2-4 independent clones after transformation with verified unique barcodes were kept and used in the competition experiment as biological replicates and termed unique "strain-BC". Prior to the experiment, all strains were streaked out and single colonies of each strain type and barcode were picked and grown overnight to saturation. The following morning, 5 μL of the overnight culture for each strain was mixed together thoroughly before back-dilution into fresh conditioned MCCG media with specified inducer concentration (see 'Media' for details). Eight concentrations of inducer (IPTG) was tested: 10, 15, 20, 25, 30, 40, 70, and 500 μM. When the culture reached OD_{600} = 0.1, 156 μL of culture was transferred to 10 mL fresh, pre-warmed, shaking conditioned MCCG to continue exponential growth (1/64 or 2^6 back-dilution). The remainder of the cells were spun down at 4°C, decanted of media and immediately frozen for eventual DNA extraction. Subsequently, when cells again reached OD_{600} = 0.1 another back-dilution was performed and cells were frozen for DNA. This process continued until reaching roughly 40 generations total. Due to the extensive experiment time some later rounds of back-dilution were decreased (312.5 or 625 μL OD_{600}=0.1 culture into 10 mL fresh culture: 1/32 or 1/16 back-dilution). This decrease in generation time was noted during quantification & final analysis.

To generate amplicons for sequencing and barcode counting frozen cell pellets were first thawed and resuspended in 480 μL 50 mM EDTA and 120 μL 10 mg/mL lysozyme. Genomic DNA was harvested using the Wizard Genomic DNA Purification Kit (Promega) according to the manufacturers protocol for Gram Positive Bacteria. Barcode amplicons were created using a two round PCR protocol. During the first round of PCR (4 cycles), primers added specific "timepoint bar codes" for multiplexing, 17 random nucleotides for collapsing PCR duplicates, and partial Illumina sequencing adaptors. Samples were pooled by induction condition and cleaned up using Select-a-Size DNA Clean & Concentrator columns (Zymo). During the second round (12-16 cycles), full Illumina sequencing adaptors were added using standard library prep primers (o231 & indexing primers). Illumina indices were used to differentiate samples on the sequencer. Final PCR products were run on an 8% TBE gel (Novex) for size selection, excised, extracted, and precipitated. Libraries were sequenced on an Illumina HiSeq 2000 or NextSeq500. For a list of primers see Table S2 and for details on amplicon structure and barcodes see Table S4.

Please cite this article in press as: Parker et al., Growth-Optimized Aminoacyl-tRNA Synthetase Levels Prevent Maximal tRNA Charging, Cell Systems (2020), https://doi.org/10.1016/j.cels.2020.07.005

QUANTIFICATION AND STATISTICAL ANALYSIS

Fitness Calculation

The method to calculate the fitness of strains during the competition experiment is as follows. First, sequencing reads were checked for correct amplicon structure, matched to the appropriate experiment, timepoint, barcode, and duplicates in the 17N random region were collapsed. At each timepoint, the $\log_2$ ratio of the counts of each strain-BC to the average counts of the four strain-BC strains for the 'no insert control' strain-type was calculated. The 'no insert control', is a strain derived from wildtype 168 with an insertion at the *amyE* locus including the pSpankHY promoter system and spcR resistance gene similar to the inducible aaRS constructs. However, instead of a protein-coding open reading frame inserted under the pSpankHY promoter, the ORF was removed and no protein product was produced (hence 'no insert'). This strain was then barcoded with the barcoding plasmid (*lacA*::BC-tetM) producing four independent strain-BC biological replicates of this strain-type. This strain-type was used as the point of comparison to control for the addition of antibiotic markers and deletion of *amyE* ORF. This control showed a ~1% growth defect compared to wildtype at all induction levels. After calculating the $\log_2$ ratio for each timepoint for a given strain-BC, the slope of the linear regression of this ratio over the number of generations of the full experiment was then calculated. The number of generations was calculated as the number of doublings of the wildtype since the prior backdilution (20 minute per doubling). In general, a 64-fold backdilution was used and therefore 6 generations had passed since the previous timepoint. When the backdilution was reduced (32-fold or 16-fold) the number of generations from the previous timepoint was adjusted accordingly (5 or 4 respectively). The fitness for the strain-BC was then computed as 1 + slope. The fitness of the 2-4 strain-BC of each strain-type was then averaged to report the final fitness for that strain-type. The fitness difference between all pairwise comparisons of strain-BCs of equivalent strain-type is plotted as a distribution to demonstrate strain-BC "biological" noise in Figure S1B.

In our analysis, we found a floor of read counts for each strain-BC of around 200 reads, potentially due to PCR crosstalk, which could skew the calculated fitness. For example, if the slope of the linear regression was calculated over all timepoints for a particularly unfit strain, this read count floor would artificially decrease the slope and artificially increase the fitness calculated. To circumvent this problem, we only considered generation timepoints prior to the first timepoint with <200 reads when calculating the slope of the linear regression. For particularly unfit strains such as low induction of *leuS*, this meant the slope and fitness were calculated with the first two or three timepoints. We also noticed that two timepoints in some induction experiments (40 μM Timepoint 1, 20 μM Timepoint 0) had extremely low read counts across all strain-BC. We attribute this to loss of DNA during collection or a failed PCR reaction in amplicon preparation. To circumvent this problem, we simply removed the affected timepoint from the slope calculation, calculating using the remaining times that passed the read floor threshold.

Calibration of aaRS Production

Protein production from the ectopic locus was estimated by first performing ribosome profiling for each aaRS strain fully induced with IPTG (500 μM), which showed limited expression changes except for the induced aaRS. The fully induced aaRS production rate relative to the rest of the cell, as measured by ribosome footprint density, was compared to that in the wildtype strain 168. At other IPTG concentrations, aaRS production relative to the fully induced situation was calibrated by the relative promoter strength, which we measured by qRT-PCR for an independent strain that has the same inducible promoter (pSpankHY) driving *gfp* expression from the same *amyE* locus. For example, ribosome profiling data showed that the level of IleS production at full induction is 14-fold higher than in wildtype cells. At 40 μM IPTG, the promoter activity, determined from RT-qPCR of the *gfp* construct, is 9.4-fold lower than at 500 μM, meaning that IleS production is inferred through calibration to be 1.5-fold higher than the wildtype level.

This calibration provides an estimate for the relative promoter strength compared to the wildtype level and should not be taken as an absolute measure of expression levels. Because aaRS production affects growth and growth affects global gene expression even for a constitutive promoter (Klumpp et al., 2009; Liang et al., 1999; Zhu and Dai, 2019), we expect the absolute output of the promoter to vary with aaRS production. Although our ribosome profiling data could be used to empirically measure the aaRS expression at different IPTG concentrations, such an analysis is limited to providing the expression relative to other genes, which themselves are affected by growth rate changes. For example, a low IPTG concentration not only reduces aaRS production, but also leads to reduced global gene expression. Indeed, in this case, the apparent 'knockdown' in aaRS as a fraction of protein synthesis (as measured by ribosome profiling) is less than the calibrated fold-change in promoter strength from the wildtype level because most other genes have reduced expression (Figure S6A). If the fitness landscape is plotted for aaRS production in terms of fraction of protein synthesis instead of calibrated promoter strength, this would lead to an artificially sharper fitness cliff at underproduction (Figure S6B), although in reality the promoter is much more repressed than the apparent knockdown. We therefore chose to report the calibrated production to avoid such confounding effects.

Ribosome Profiling and RNA-seq Data Analysis

Processing of ribosome profiling sequencing reads included removal of the linker sequence and mapping with Bowtie (Langmead et al., 2009) (options -v 2 -k 1) to the NC_000964.3 reference genome obtained from NCBI Reference Sequence Bank. Footprint reads with sizes between 20 to 40 nucleotides were stripped of the first and last 8 nucleotides and a count of 1/n where n equals the remaining read length was assigned to the remaining positions. To calculate proteome fractions for regulons, the total read counts for a subset of genes in the regulon was compared to all ORF mapping reads excluding start and stop codons. Processing of RNA sequencing reads included removal of PolyA tails and mapping with Bowtie (Langmead et al., 2009) (options -v 2 -k 1) to the

Please cite this article in press as: Parker et al., Growth-Optimized Aminoacyl-tRNA Synthetase Levels Prevent Maximal tRNA Charging, Cell Systems (2020), https://doi.org/10.1016/j.cels.2020.07.005

NC_000964.3 reference genome. The five prime ends of reads mapping to open reading frames was counted excluding the first and last five positions. Read counts were normalized by total mapped reads and gene length (RPKM) or total mapped reads (RPM).

The average ribosome occupancy at the 61 sense codons was computed by first normalizing read counts at each nucleotide in a coding sequence by the mean read count for that sequence (excluding the first and last 15 nucleotides) using the Ribosome profiling data. This normalized ribosome occupancy was averaged across the three nucleotides of each codon, and then averaged across all occurrences of that codon within the coding region. Final values were computed by averaging across all coding sequences meeting a threshold of five sequencing reads per nucleotide. Only genes reaching this threshold in all compared experiments were considered in the final analysis. Ribosome queuing was calculated by similarly normalizing read counts at each nucleotide in a coding region by the mean read count for that region. For each instance of a codon, a window of 100 nucleotides upstream and downstream of the second codon position were obtained and windows were averaged across all instances of the codon within that gene. Only codons over 115 nucleotides away from a start and stop codon were considered. Final values were computed by averaging across all coding sequences meeting a threshold of five sequencing reads per nucleotide. For comparison between experiments, the average density at each position in the window from the wildtype was subtracted from the average density in the SerS underproduction experiment.